Atomic placement of Al on the GaAs {001} $c(4\times4)$ reconstruction determined by angle-resolved secondary-ion mass spectrometry

Stephen H. Goss,* Gregory L. Fisher, Prasad B. S. Kodali,† Barbara J. Garrison, and Nicholas Winograd
Department of Chemistry, The Pennsylvania State University, University Park, Pennsylvania 16802
(Received 14 July 1998)

The atomic structure of the initial Al/GaAs {001} $c(4\times4)$ interface has been examined by angle-resolved secondary-ion mass spectrometry. We find that Al atoms adsorb to second layer As atoms and do not disrupt the surface reconstruction up to 1.0 ML of deposited Al when prepared *in situ* via molecular beam epitaxy. The Al atoms are found not to adsorb to first layer As atoms and do not dimerize on this surface. The structure is determined by comparing angular distributions of Al^+ and Ga^+ ions to molecular-dynamics simulations of the ion bombardment event. [S0163-1829(99)03716-9]

I. INTRODUCTION

Identifying the structure of reconstructed GaAs {001} surfaces has been pursued for years[1–3] due to its importance as a material for use in high-speed electronics, lasers, and photodetectors.[4–8] Paramount to realizing the use of GaAs as a standard semiconductor in such applications is the task of relating surface and interface structure to the affected electrical properties. This goal is complicated by the presence of large surface unit cells with manifold atomic structures and compositions. Indeed, slight variations in molecular beam epitaxy (MBE) growth conditions, or decapping of As-capped surfaces for *ex situ* analysis, have a pronounced effect on surface reconstruction and morphology. These entanglements, together with the complex reactivity of GaAs with metals and other semiconductors, have made structural analysis difficult and have limited design of metal-semiconductor interfaces with prescribed electrical properties.[9–12]

For clarity, a brief overview is given here to substantiate the clean, reconstructed GaAs {001} surface, upon which we have deposited Al, employed during our *in situ* experimental studies. Most research on GaAs {001} surfaces has focused on the (2×4) reconstruction,[13–20] but a large body of information regarding the $c(4\times4)$ reconstruction has been gathered as well.[13–17,21–25] Studies on the $c(4\times4)$ reconstruction reveal that the surface is composed of dimers bound in the $\langle011\rangle$ direction with a bond length of 2.69 ± 0.10 Å.[22,23] It is generally accepted that the GaAs {001} $c(4\times4)$ reconstruction is terminated with two layers of As with the top layer containing As dimers and the second layer containing a full layer of As,[13–16,21–25] although one study suggests that the second layer is composed of a mixture of Ga and As.[17] A layer-compressed diagram of the $c(4\times4)$ reconstruction is shown in Fig. 1. As indicated by the figure, there is some disagreement within the literature on the number of surface dimers present. We have determined, using reflection high-energy electron diffraction (RHEED) and secondary-ion mass spectrometry (SIMS), that our MBE growth procedure consistently yields a two-dimer $c(4\times4)$ reconstruction for subsequent use in Al deposition experiments.[25]

Metal deposition on semiconductor surfaces represents a major thrust in current research, much of which has focused on the structure-property relationships of Al/GaAs. A key to understanding these relationships is the interfacial bonding that occurs between deposited Al and the GaAs surface. Studies conducted on Ga-rich GaAs {001} surfaces show Al to react with GaAs disrupting the surface, while on As-rich surfaces there appears to be no interfacial disruption.[26,27] Upon initial deposition of Al [$\leqslant$1 monolayer (ML)] onto As-rich surfaces, metal islands are observed to form in the dimer rows[28] followed by three-dimensional nucleation at approximately 3 ML of deposited Al.[26] As the deposition progresses, Al nucleation results in formation of (001) and mixed (001)/(011) crystallites.[26,28–32] At thick Al coverages the (001) and (011) domains are observed to coalesce forming single-crystal Al(001). It has also been reported that high rates of deposition result almost exclusively in Al(001) nucleation.[30–32] Hence, there are both kinetic and thermodynamic components to Al nucleation on GaAs {001} surfaces before the thermodynamically favored single-crystal growth of Al(001) dominates.[26,28–31,33,34]

In spite of this wealth of data, a comprehensive model of Al nucleation on GaAs {001} has not yet been reported. This, presumably, is due to a lack of detailed information regarding Al/GaAs {001} interfacial bonding, and is exacerbated by a wide range of preparative techniques that incorporate varying degrees of (001) and (011) domains via defects.[26,28–32] Recently, though, theoretical studies have been employed to investigate interfacial Al(001)/GaAs {001} bonding as a means of developing a model to predict Schottky barrier characteristics.[33,34] It was reported that the lowest-energy state is an abrupt interface, incorporating a four atomic-layer relaxation region, where Al forms short, covalent bonds to As. The predicted Schottky barrier heights, based on this model, are in excellent agreement with those determined by experiment.

We report here Al/GaAs {001} $c(4\times4)$ interfacial bonding of the type predicted by theory.[33,34] Using SIMS, we have measured the angular distributions of desorbed Al^+ and Ga^+ ions. These distributions, in conjunction with molecular-dynamics (MD) simulations, lead to the identification of desorption mechanisms and reveal how these desorption mechanisms change with the addition of Al overlay-

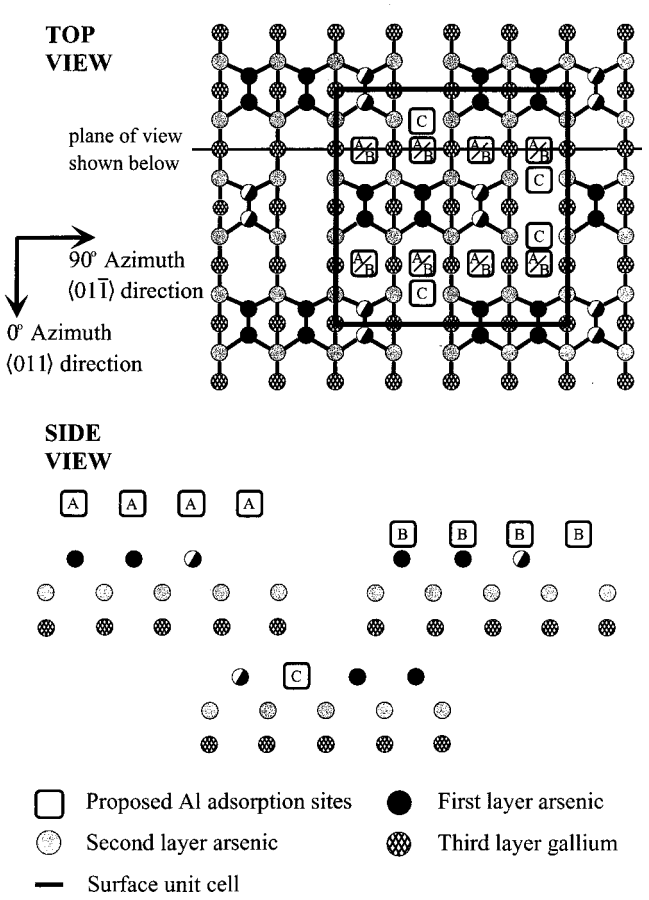

FIG. 1. The proposed surface structure of the GaAs {001} $c(4\times4)$ surface. The top view is layer compressed showing the first three layers of atoms. The half-shaded As atoms are only present in the three-dimer model. The three adsorption sites of Al on the $c(4\times4)$ surface, discussed in this paper, are indicated with squares. Site A is between the dimers at a height of 1.6 Å above the dimers. Site B is between the dimers at a height of 0.8 Å above the dimers. Site C is at the same height as the As dimers in a bulk epitaxial position. In each case the side view is along the $\langle 01\bar{1}\rangle$ ($\Phi=90°$) azimuth, and all planes of atoms are shown.

ers. By identifying the desorption mechanisms that give rise to peaks in the distribution, and tracking those peaks with each Al deposition, we can qualitatively identify the atomic position of adsorbed overlayers. The adsorption site for Al deposited onto GaAs {001} $c(4\times4)$ at a coverage of 0.33 ML is found to be at about the same height as the first-layer As dimers, bound to second-layer As atoms. Upon deposition of 1.0 ML, Al maintains adsorption sites congruent with the 0.33 ML adsorption sites and does not disrupt the original GaAs {001} $c(4\times4)$ reconstruction. These results are consistent with STM,[28] RHEED, and Auger[26] studies, conducted at low Al coverages ($\leqslant$1 ML), where deposited Al is observed to form metal islands in the dimer rows and did not disrupt the initial surface reconstruction.

II. EXPERIMENT

The equipment required to perform these angle-resolved SIMS experiments on GaAs {001} surfaces is inherently complex[35,36] and has been modified significantly since its inception. Samples were prepared in a commercial Riber 2300 MBE chamber that is lined with liquid N_2 shrouds, evacuated with a 500 l/s ion pump, a titanium sublimation pump, and a 3700 l/s cryogenic array pump. The chamber is equipped with a 10 keV RHEED system used to monitor surface conditions and growth rate *in situ*. A residual gas analyzer is present to monitor background gas conditions.

The GaAs {001} samples were prepared from two-inch intrinsically doped wafers obtained from M/A COM Laser Diode Inc. and American Xtal Technology. Prior to insertion into the UHV system, the samples were spin etched with a 10:1:1 solution of H_2O, H_2O_2, and NH_4OH for 30 sec, then rinsed with deionized H_2O, dried with N_2, and mounted on Mo blocks with In. After insertion into the ultrahigh vacuum preparation chamber, samples were degassed at 650 K for 3 h, then inserted into the MBE chamber and degassed at 900 K under a heavy As flux for 1 h to remove any remaining surface oxides.

Growth of GaAs films was performed at a temperature of 880 K with an elemental flux ratio of $\sim$5:1 [As_4]/[Ga] as measured by a nude ion gauge. Growth rates of $\sim$0.8 μm/h were measured by RHEED oscillations. 4-μm buffer layers were grown on new crystals to generate a pristine surface before Al was deposited and SIMS analysis performed. An additional 0.5-μm layer of GaAs was deposited between experiments to regenerate the pristine surface. It is known that slight variations in [As_4]/[Ga] flux ratio and sample temperature upon termination of growth lead to very different surface reconstructions.[22,25,27] To eliminate variations in the surface reconstruction a systematic process was developed to grow a reproducible $c(4\times4)$ reconstruction. Our procedure was to terminate the Ga flux while the sample was at growth temperature, then reduce the As flux by a factor of 10 by lowering the As cell temperature while simultaneously reducing the sample temperature to 650 K. At this point the RHEED pattern indicates a $c(4\times4)$ reconstruction. The surface is held at this temperature under As flux for 30 min to ensure thermal equilibrium, then the As flux is terminated and the sample temperature is reduced to room temperature. This procedure gives a well-defined $c(4\times4)$ RHEED template to which subsequent Al layers were added.

Aluminum growth rates were measured by RHEED oscillations where one oscillation equals 6.24×10^{14} atoms/cm^2, which corresponds to one layer of AlAs. The deposition rate of Al was 0.067 ML/s on the $c(4\times4)$ surface. After deposition of 0.33 ML of Al, the RHEED pattern maintained a $c(4\times4)$ periodicity that was slightly attenuated relative to the clean surface. After deposition of 1.0 ML of Al, the RHEED pattern maintains the $c(4\times4)$ periodicity with no half-order streaks in either the $\langle 011\rangle$ or $\langle 01\bar{1}\rangle$ directions. The samples were then transferred under UHV into the analysis chamber where angle-resolved SIMS measurements were performed.

A full angle-resolved scan is obtained by first setting energy and mass of the ions desired, and collecting an azimuthal scan at a desired detector angle. This is repeated for several detector angles. Each azimuthal scan is obtained by fixing the detector angle (Θ_D) while rotating the azimuthal angle (Φ) two or three times. The polar angle (Θ_p) is defined as the angle between the sample normal and the ray extend-

ing from the detector to the surface. The value of Φ is defined by the angle produced by rotating the sample relative to a starting reference point (i.e., $\Phi = 0°$, 180°, and $\langle 011 \rangle$ are azimuthal equivalents, see Fig. 1). Multiple azimuthal rotation is used to monitor ion beam damage and provides a convenient method for signal addition. In each of the azimuthal scans, the sample was kept normal to the ion beam to minimize any effects caused by the ion beam interacting with near-surface atoms in the lattice along a specific direction as the sample is rotated causing preferential desorption in that direction.[22] A polar scan is taken by fixing Φ while moving the detector relative to the sample. A minimum of three polar scans were taken and added to create an averaged polar scan, which is used to normalize the set of azimuthal scans for a given energy.

Ion desorption is generated by a 3 keV beam of Ar^+ ion at ~2 nA focused to a 2-mm diameter spot on the crystal. The total ion dose on the surface never exceeds 3×10^{13} ions/cm^2 throughout the entire experiment. Only Ga^+ and Al^+ ions are detected in these experiments due to the low yield of As^+ and As^- ions. The only way to obtain a suitable ion yield for As is to increase the ion current by a factor of 10^3, which causes too much surface damage and eliminates any crystal information from the surface. By maintaining the low primary ion dose, surface structural integrity is maintained.

III. EXPERIMENTAL RESULTS AND DISCUSSION

The proposed structure of the GaAs {001} $c(4\times4)$ surface is shown in Fig. 1. This figure shows the preferred structure of the $c(4\times4)$ surface determined by STM[13,14,21] and grazing-incidence x-ray diffraction.[15,23] The three-dimer surface does fit the bonding requirements for semiconductor surfaces based on the simple electron counting rules, while the two-dimer surface does not completely fit this model.[37] Previous studies suggest that the two-dimer $c(4\times4)$ reconstruction is the surface produced during these experiments.[25] The number of dimers on the surface does not affect the number of proposed Al adsorption sites on the $c(4\times4)$ surface for sites A and B, but does affect the number of Al sites for site C. The number of proposed Al adsorption for sites A and B is 0.5 ML, or 3.13×10^{14} atoms/cm^2. The removal of one dimer will double the number of Al adsorption sites from 0.25 to 0.5 ML for site C.

The experimental angular distributions of the 8 eV Ga^+ ions from the clean $c(4\times4)$ reconstruction, and following deposition of 0.33 and 1.0 ML of Al, are shown in Fig. 2. Due to the symmetry of the $c(4\times4)$ surface, we will only discuss the features between $\Phi = 90°$ and 180° in the experimental and theoretical data. Each one of the scans shows a highly anisotropic distribution, typical of Ga^+ ions from GaAs {001} surfaces.[35,36] These scans also show how the Ga^+ ion distribution changes with changing Al coverage. The clean $c(4\times4)$ distribution, shown in Fig. 2(a), reveals three peaks in the distribution. The dominant peak is at $\Phi = 90°$ and is labeled 1, while the two minor peaks in the distribution are positioned at $\Phi = 125°$ and 180° and are labeled 2 and 3, respectively. The desorption mechanisms that lead to the formation of these peaks have been detailed in previous papers.[22,25,27] Briefly, the largest peaks arise by direct collision between fourth-layer As and third-layer Ga causing Ga^+ ion ejection along the common bond direction. Features at higher polar angles arise from a mix of mechanisms related to the missing As atoms in the reconstructed surface.

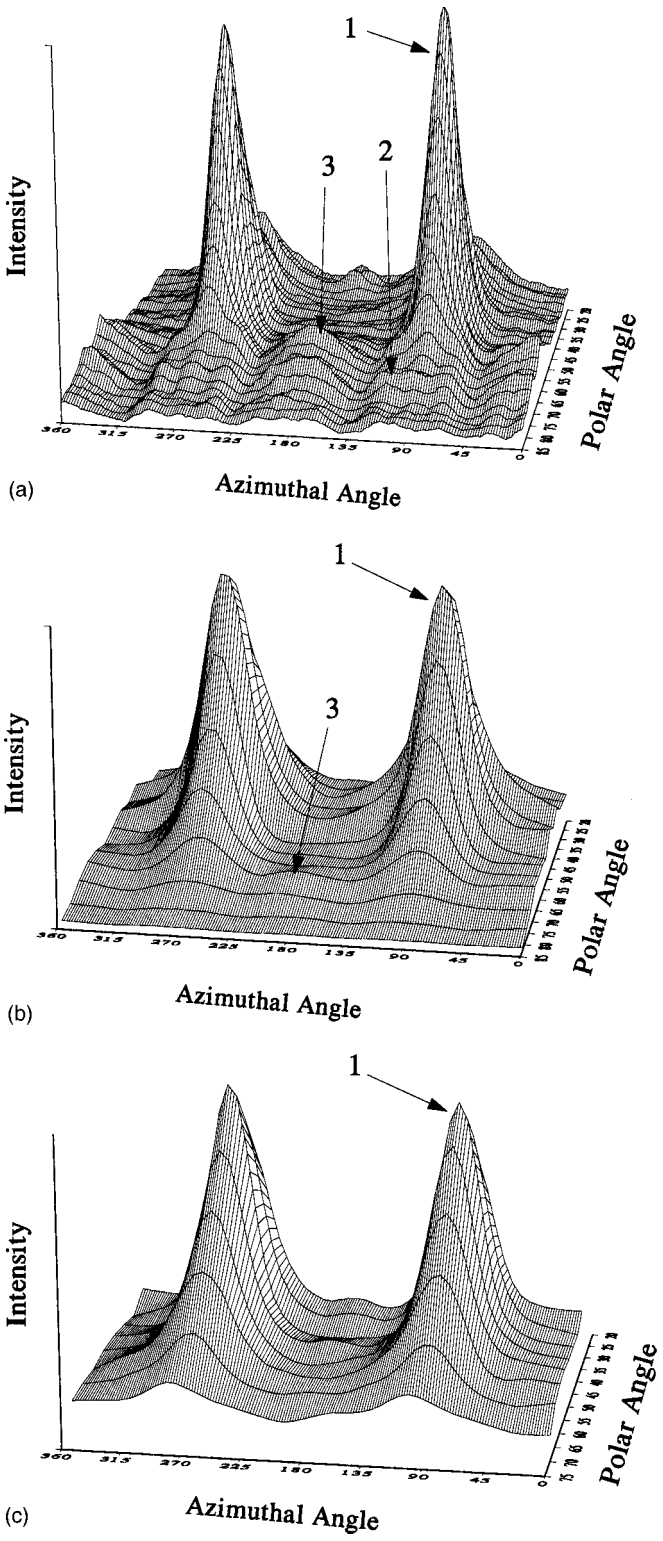

FIG. 2. The angular distributions of 8 eV Ga^+ ions from: (a) the clean GaAs {001} $c(4\times4)$ surface, (b) 0.33 ML of Al deposited at room temperature on the $c(4\times4)$ surface, and (c) 1.0 ML of Al deposited at room temperature on the $c(4\times4)$ surface. The arrows show the major ejection peaks in the distribution.

At 0.33 ML of deposited Al the intensity of peak 1 remains dominant, the intensity of peak 2 has decreased to zero, and the intensity of peak 3 is diminished significantly, as shown in Fig. 2(b). At 1.0 ML of deposited Al, peaks 2 and 3 are missing and only peak 1 remains in the distribution, shown in Fig. 2(c). This result indicates that the Al is preferentially adsorbing to sites that would not attenuate peaks 1, 2, and 3 equally.

The angular distributions of 8 eV Al^+ ions are shown in Figs. 3(a) and 3(b). These figures reveal only a single peak in each of the distributions. These peaks are very different from angular distributions of diamond-lattice crystals in that they are very wide azimuthally. Typically, narrow peaks have been observed in distributions from semiconductors because a major ejection mechanism is nearest-neighbor collision along the bond direction.[25,36] Broader distributions have been observed more frequently for metal systems in which the collision cascade is not dominated by such highly directional motion.[38–40] The wide Al^+ distribution in Figs. 3(a) and 3(b) indicates that directional focussing is not taking place and, therefore, Al is most likely adsorbing on the surface and is not incorporated into the bulk. In Fig. 3(c) the angular distribution of 12 eV Al^+ ions reveals two different peaks. The position of the major peak, labeled 1, is at $\Phi = 90°$ and the position of the secondary peak, labeled 2, is at $\Phi = 115°$. When the Al coverage is increased from 0.33 to 1.0 ML the angular distribution does not change significantly, as observed in the distributions of Figs. 3(a) and 3(b). This result indicates that Al adsorption above 0.33 ML coverage is similar to adsorption below 0.33 ML.

The polar scans, at $\Phi = 90°$, of Al^+ ions at 0.33 ML coverage on the $c(4\times4)$ reconstruction at different energies are shown in Fig. 4. At the highest energy, 12 eV, the polar distribution peaks at 45° and is relatively narrow. For 8-eV ejection the peak is at 50°, while 4-eV ejection peaks at 55° and is significantly broader. This trend of shifting polar angle with energy is indicative of the ejected particle being drawn towards the surface by an attractive interaction.[41,42]

Changes in the Al^+ ion polar distributions versus Al coverage are shown in Fig. 5(a). Both Al^+ ion polar scans have a maximum at a polar angle of 50°, but the distribution at 0.33 ML Al coverage has a greater intensity at high polar angles while the distribution at 1.0 ML Al coverage has greater intensity at low polar angles. This intensity shift to low polar angles with an increase in Al coverage suggests that additional Al binds close to the initial Al site yielding a metal-like distribution.

The 8 eV Ga^+ ion signal in the polar scans, shown in Fig. 5(b), reveals a maximum at 50° for the clean surface that decreases to 45° at 0.33 and 1.0 ML Al coverages. The meager peak shift in the Ga^+ ion distribution indicates that Al adsorbs to sites on the $c(4\times4)$ surface which do not strongly influence Ga^+ ion desorption. If Al atoms were adsorbing in sites A or B, which are in the same plane as desorbing third-layer Ga atoms, the Ga^+ ion distribution would be more focused by the overlying Al atoms resulting in a more anisotropic Ga^+ ion distribution. Since Al adsorption only slightly influences the Ga^+ ion distribution, it is likely that Al adsorbs to site C, which is not in the desorption plane of third-layer Ga atoms.

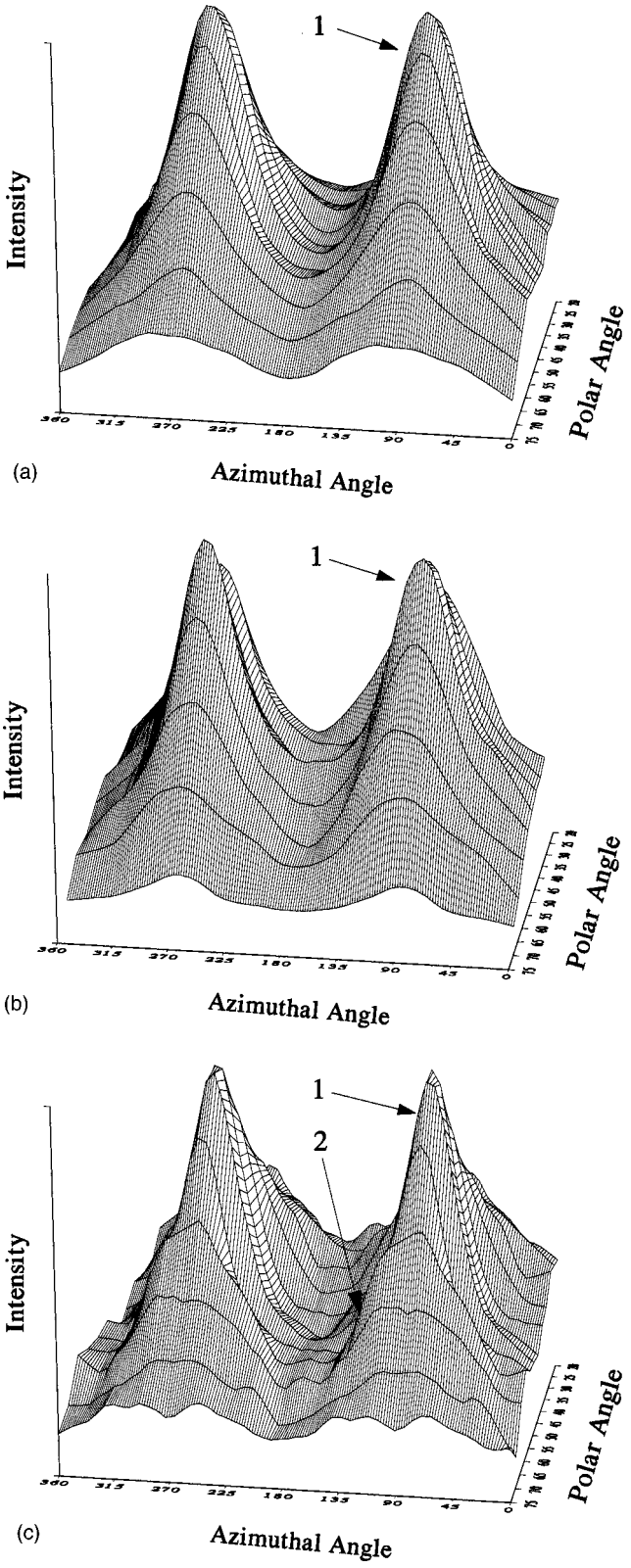

FIG. 3. (a) The 8 eV Al^+ ion angular distribution at 0.33 ML Al coverage. (b) The 8 eV Al^+ ion angular distribution at 1.0 ML Al coverage. (c) The 12 eV Al^+ ion angular distribution at 0.33 ML Al coverage.

IV. THEORETICAL RESULTS AND DISCUSSION

Molecular dynamics simulations of the keV bombardment process are useful in determining desorption mechanisms

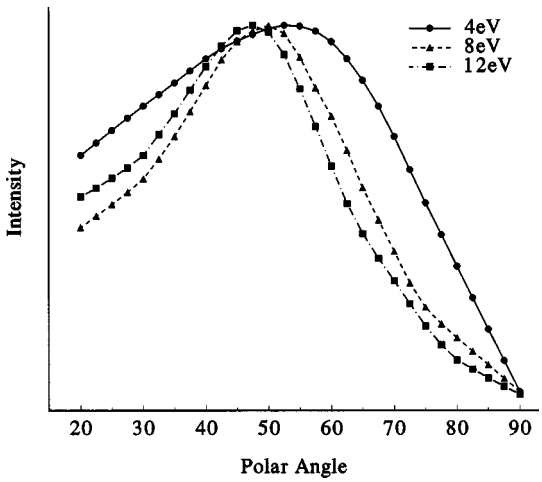

FIG. 4. The polar distribution of Al^+ ions from the $c(4\times4)$ surface at 0.33 ML Al coverage. The figure shows how the distribution changes with desorption energy. The intensity at $\Theta_p = 90°$ is zero.

from crystalline solids.[38,41,43] In particular, detailed mechanistic study has shown that atoms in a diamond lattice eject via two primary mechanisms. First, the closest atom in the layer just below the surface layer may cause desorption via nearest-neighbor collision (Δ_1 mechanism). Second, an atom from three layers below the surface layer may move unimpeded through the crystal lattice and cause desorption of a first-layer atom (Δ_3 mechanism). The computational procedure is presented elsewhere and the interested reader should refer to those papers for a more complete overview of the MD calculations performed.[38,42,44]

MD calculations with a Si potential energy surface (PES) were used in this paper to identify desorption mechanisms and to relate the angular distributions to the Al adsorption sites on the surface. It has been shown in previous studies that the Si PES adequately, though only qualitatively, describes the angular distributions of GaAs and Al/GaAs systems because the desorption mechanisms are more dependent on atomic positions than on mass or chemical environments of the atoms in the lattice.[25,27,35,36,41,45]

Three different Al adsorption sites on the $c(4\times4)$ reconstruction, shown in Fig. 1, were modeled with MD calculations using a Si {001} $c(4\times4)$ reconstruction to identify desorption patterns of adsorbate and surface atoms. The reason these three sites were chosen as proposed Al adsorption sites for the $c(4\times4)$ reconstruction is that these sites have high-electron density from lone pairs of electrons on the surface As atoms. The two different heights above the surface for sites A and B were chosen for two reasons: one reason was to match the previous (2×4) experiments,[27] and the second reason was that the $c(4\times4)$ reconstruction is found to have tilted dimers.[22] Sites A and B are antiepitaxial growth sites for the $c(4\times4)$ reconstruction. Site C, however, is an epitaxial growth site for the $c(4\times4)$ reconstruction.

A Si crystal ten layers deep with 256 atoms per layer was employed for the MD simulations. A layer of 128 atoms was used to represent the surface reconstruction. A subsequent 128 atoms representing the Al adlayer was added to the lattice and placed in position A or B. For position C 256 atoms were used in the top layer. An approximation is needed to describe the desorption results from site C since adsorbed Al atoms and first-layer As atoms are equiplanar. Such a construct was achieved by subtracting the angular distribution intensity of the Al-free surface from that of the surface with the Al adlayer atoms. The presence of adatoms alters the path of first-layer atoms from their clean-surface desorption trajectories introducing some error. Previous papers, however, have shown that these errors are small.[41]

The MD results for Al desorption from sites A and B are shown in Figs. 6(a) and 6(b), respectively, for kinetic energies of 3–10 eV. Both of these angular distributions indicate that the dominant peak is at $\Phi = 180°$. The angular distribution in Fig. 6(a) has a wider azimuthal distribution than the distribution in Fig. 6(b), but both sets of results are qualitatively similar. The formation of the peaks at $\Phi = 180°$ is caused by first-layer As striking an Al atom along the common bond (Δ_1 mechanism) ejecting the Al atom in that direction. Both of these scans are different from the experimental results shown in Fig. 3, which yield a dominant peak at $\Phi = 90°$.

The MD angular distributions of Al adsorbed in site C are

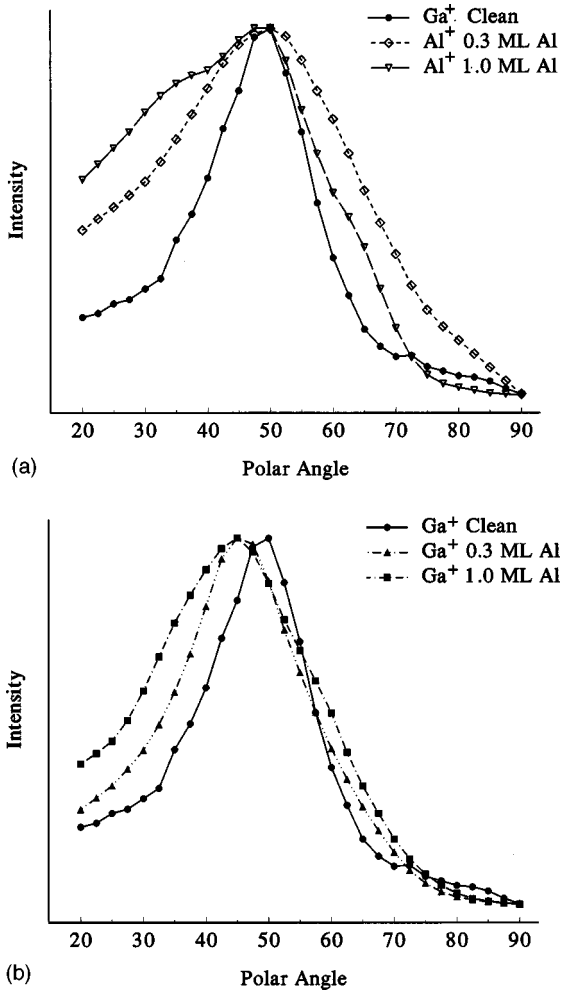

FIG. 5. (a) The polar distribution of Al^+ ions from the clean $c(4\times4)$ surface, and following deposition of 0.33 ML and 1.0 ML of Al. (b) The polar distribution of Ga^+ ions from the clean $c(4\times4)$ surface, and following deposition of 0.33 ML and 1.0 ML of Al. The polar distributions show how adsorption of Al influences the Ga^+ and Al^+ ion distributions. Intensities at $\Theta_p = 90°$ are zero.

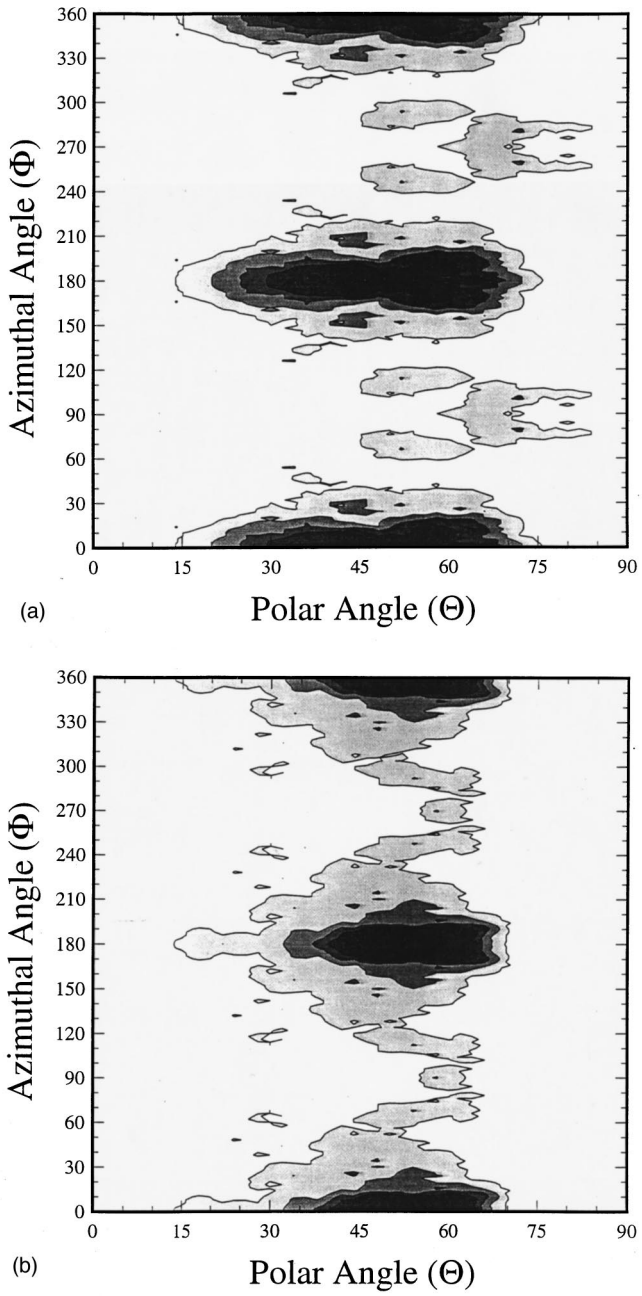

FIG. 6. (a) The theoretical angular distribution of Al^+ ions from site A. (b) The theoretical angular distribution of Al^+ ions from site B. The energy range of each scan is 3–10 eV.

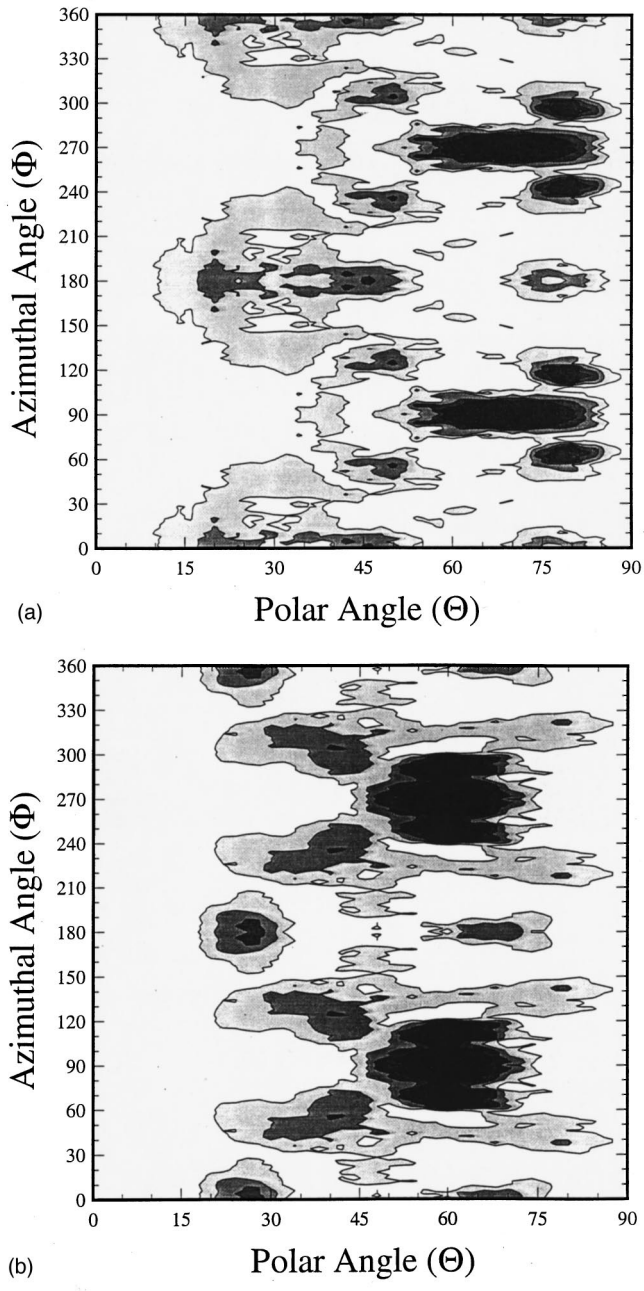

FIG. 7. (a) The theoretical angular distribution of 0–10 eV Al^+ ions from site C. (b) The theoretical angular distribution of 10–20 eV Al^+ ions from site C.

shown in Figs. 7(a) and 7(b) for 0–10 and 10–20 eV particles, respectively. Both of these distributions are characterized by a dominant peak at $\Phi = 90°$, formed by second-layer As striking an Al atom along the common bond (Δ_1 mechanism) ejecting the Al atom in that direction. These distributions also illustrate that the polar angle shifts to lower values as the desorption kinetic energy increases. This peak shift is due to an attractive surface potential at low desorption energies. The same shift was observed for the experimental results, as shown in Fig. 5(a). The Al atom distribution shown in Fig. 7(b) for the 10–20 eV desorption energy is characterized by a broad peak in the azimuthal distribution. This peak is actually composed of three peaks, one at $\Phi = 90°$, and two lesser peaks at $\Phi = 70°$ and 110°. These results are qualitatively similar to the experimental results shown in Fig. 3.

By comparing the experimental angular distributions to MD simulation distributions, we have deduced the most likely initial adsorption site for Al deposited onto the GaAs {001} $c(4\times4)$ reconstruction to be an epitaxial site in the lattice where Al is bound to As in the second layer (site C in Fig. 1). The adsorption site for Al on the $c(4\times4)$ surface is different from the adsorption site for Al on the GaAs {001} (2×4) surface.[27] For the GaAs {001} (2×4) surface, Al adsorption was determined to be between the rows of As dimers at a height of 0.79 ± 0.1 Å above the surface dimers. This difference in Al adsorption sites is due to the electron lone-pair configuration between the (2×4) and $c(4\times4)$ re-

constructions. The electron configuration of the (2×4) reconstruction is such that there are only lone pairs of electrons on the surface As atoms along the $\langle 01\bar{1}\rangle$ azimuth. Thus, Al can only adsorb to those lone-pair sites. The $c(4\times4)$ reconstruction has an electron configuration that allows lone pairs of electrons in both the first and second layers.[19] The lone pairs from the second-layer As in the $c(4\times4)$ reconstruction are pointing along the $\langle 01\bar{1}\rangle$ ($\Phi=90°$) azimuth while lone pairs from the first-layer As dimers are pointing along the $\langle 011\rangle$ ($\Phi=180°$) azimuth. One reason why Al atoms preferentially adsorb to the lone pairs along the $\langle 01\bar{1}\rangle$ ($\Phi=90°$) azimuth is that Al would prefer to form strong bonds with As. To form a strong bond the Al atom needs to be positioned relatively close to its As neighbor, which favors bonding with As lone pairs that lie in the $\langle 01\bar{1}\rangle$ ($\Phi=90°$) direction.

Comparison of the 0.33 ML coverage state to the 1.0 ML coverage state shows that Al is not adsorbing to sites A or B after site C are filled because there is no Al^+ ion desorption observed along the $\Phi=180°$ direction at 1.0 ML coverage, as shown in Fig. 3(b). The similarity of Figs. 3(a) and 3(b) suggests that Al deposited above 0.33 ML adsorbs to sites congruent to site C in the rows of As dimers and begins to cluster forming Al metal islands. A possible reason why the Al does not bond to sites A or B may be related to the antiepitaxial nature of these sites. The third-layer Ga atoms induce a partial negative charge in the second-layer As atoms. If Al atoms were to adsorb to sites A or B, a partial negative charge would be induced in the first-layer As atoms. This would produce two partial negative charges one layer apart, resulting in simple Coulomb repulsion. More advanced computer simulations of Al metal growth on GaAs surfaces are awaiting the development of an improved potential-energy surface to follow up this study.

V. CONCLUSION

The essential structure of the Al/GaAs {100} $c(4\times4)$ interface formed at room temperature is proposed. The Al adsorption site on the $c(4\times4)$ surface is found to be in epitaxial sites bound to second-layer As atoms, not first-layer As dimers. This is in contrast to Al adsorption on the GaAs {100} (2×4) surface where Al was found to adsorb to the first-layer As dimers. The reason for this difference is related to the electron lone-pair configuration differences of the two surfaces. The (2×4) surface has electron lone pairs in the troughs between the rows of As dimers, thus Al can only bind to those sites. The $c(4\times4)$ surface has two different positions for electron lone pairs on the surface and Al bonds to only one type—those that produce short, strong bonds with the surface. This experimental observation supports the theoretical model of Berthod, Binggeli, and Baldereschi,[33] and Dandrea and Duke.[34] After the epitaxial sites are filled Al is not observed to bind to first-layer As. This is supported by RHEED observations in which a $4\times$ periodicity was maintained throughout the deposition regime studied. This result, in combination with the SIMS angular distributions, suggests that deposited Al forms islands on top of the initial Al adsorption sites at coverages below 1.0 ML. It is our hope that the experimentally determined interfacial structure of Al/GaAs {001} $c(4\times4)$ presented here will aid further development of models to describe nucleation of metals on GaAs surfaces and more precisely predict Al/GaAs electronic characteristics.

ACKNOWLEDGMENTS

Financial support for this research was provided by the Office of Naval Research and the National Science Foundation.

*Present address: The Ohio State University, Columbus, OH.
†Present address: Genex Corporation, Cleveland, OH.

[1] C. B. Duke, Chem. Rev. **96**, 1237 (1996).
[2] C. Deparis and J. Massies, J. Cryst. Growth **108**, 157 (1991).
[3] A. Y. Cho, J. Appl. Phys. **47**, 2841 (1976).
[4] S. S. Li, J. Chu, and Y. H. Wang, Superlattices Microstruct. **19**, 229 (1996).
[5] C. Weisbuch, J. Vac. Sci. Technol. A **12**, 1191 (1994).
[6] W. S. Rabinovich, S. R. Bowman, D. S. Katzer, and C. S. Kyono, Appl. Phys. Lett. **66**, 1044 (1995).
[7] W. Lu, H. J. Ou, M. H. Chen, X. L. Huang, S. C. Shen, R. H. Gu, and L. B. Ye, Int. J. Infrared Millim. Waves **15**, 137 (1994).
[8] A. Thiede, M. Berroth, V. Hurm, U. Nowotny, J. Seibel, W. Gotzeina, M. Sedler, B. Raynor, K. Koehler, P. Hofmann, A. Huelsmann, G. Kaufel, and J. Schneider, Electron. Lett. **29**, 1005 (1992).
[9] C. J. Spindt, M. Yamada, P. L. Meissner, K. E. Meissner, K. E. Miyano, T. Kendelewicz, A. Herrera-Gomez, W. E. Spicer, and A. J. Arko, Phys. Rev. B **45**, 11 108 (1992).
[10] R. Duszak, C. J. Palmstrom, L. T. Florez, Y. N. Yang, and J. H. Weaver, J. Vac. Sci. Technol. B **10**, 1891 (1992).
[11] S. P. Svensson, J. Kanski, T. G. Andersson, and P. O. Nilsson, J. Vac. Sci. Technol. B **2**, 235 (1984).
[12] J. Massies, P. Devoldere, and N. T. Linh, J. Vac. Sci. Technol. **16**, 1244 (1979).
[13] T. Hashizume, Q. K. Xue, J. Zhou, A. Ichimiya, and T. Sakurai, Phys. Rev. Lett. **73**, 2208 (1994).
[14] A. R. Avery, D. M. Holmes, J. Sudijono, T. S. Jones, and B. A. Joyce, Surf. Sci. **323**, 91 (1995).
[15] V. H. Etgens, M. Sauvage-Simkin, R. Pinchaux, J. Massies, N. Jedrecy, A. Waldhauer, and N. Greiser, Surf. Sci. **320**, 252 (1994).
[16] C. Sasaoka, Y. Kato, and A. Usui, Surf. Sci. Lett. **256**, L239 (1992).
[17] J. Falta, R. M. Tromp, M. Copel, G. D. Pettit, and P. D. Kirchner, Phys. Rev. Lett. **69**, 3068 (1992).
[18] V. Bressler-Hill, M. Wassermeier, K. Pond, R. Madoudian, G. A. D. Briggs, P. M. Petroff, and W. H. Weinberg, J. Vac. Sci. Technol. B **10**, 1881 (1992).
[19] M. D. Pashley, K. W. Haberern, W. Friday, J. M. Woodall, and P. D. Kirchner, Phys. Rev. Lett. **60**, 2176 (1988).
[20] L. D. Broekman, R. C. G. Leckey, J. D. Riley, A. Stampfl, B. F. Usher, and B. A. Sexton, Phys. Rev. B **51**, 17 795 (1995).
[21] D. K. Biegelsen, R. D. Bringans, J. E. Northrup, and L. E. Swartz, Phys. Rev. B **41**, 5701 (1990).
[22] C. Xu, J. S. Burnham, R. M. Braun, S. H. Goss, and N. Winograd, Phys. Rev. B **52**, 5172 (1995).
[23] M. Sauvage-Simkin, R. Pinchaux, J. Massies, P. Calverie, N. Jedrecy, J. Bonnet, and I. K. Robinson, Phys. Rev. Lett. **62**, 563 (1989).

[24] P. K. Larsen, J. H. Neave, J. F. van der Veen, P. J. Dobson, and B. A. Joyce, Phys. Rev. B **27**, 4966 (1983).
[25] S. H. Goss, Ph.D. thesis, The Pennsylvania State University, 1997.
[26] G. Landgren, S. P. Svensson, and T. G. Anderson, Surf. Sci. **122**, 55 (1982).
[27] J. S. Burnham, D. E. Sanders, C. Xu, R. M. Braun, S. H. Goss, K. P. Caffey, B. J. Garrison, and N. Winograd, Phys. Rev. B **53**, 9901 (1996).
[28] Y. S. Luo, Y. N. Yang, J. H. Weaver, L. T. Florez, and C. J. Palmstrom, Phys. Rev. B **49**, 1893 (1994).
[29] C. J. Keiley and D. Cherns, Philos. Mag. A **59**, 1 (1989).
[30] M. Missous, E. H. Rhoderick, and K. E. Singer, J. Appl. Phys. **60**, 2439 (1986).
[31] P. M. Petroff, L. C. Feldman, A. Y. Cho, and R. S. Williams, J. Appl. Phys. **52**, 7317 (1981).
[32] J. Mizuki, K. Akimoto, I. Horisawa, K. Hirose, T. Mizutani, and J. Matsui, J. Vac. Sci. Technol. B **6**, 31 (1988).
[33] C. Berthod, N. Binggeli, and A. Baldereschi, Phys. Rev. B **57**, 9757 (1998).
[34] R. G. Dandrea and C. B. Duke, J. Vac. Sci. Technol. A **11**, 848 (1993).
[35] R. Blumenthal, S. K. Donner, J. L. Herman, R. Terhan, K. P. Caffey, E. Furman, and N. Winograd, J. Vac. Sci. Technol. B **6**, 1444 (1988).
[36] K. P. Caffey, R. Blumenthal, J. S. Burnham, E. Furman, and N. Winograd, J. Vac. Sci. Technol. B **9**, 2268 (1991).
[37] M. D. Pashley, Phys. Rev. B **40**, 10 481 (1989).
[38] S. P. Holland, B. J. Garrison, and N. Winograd, Phys. Rev. Lett. **44**, 756 (1980).
[39] N. Winograd, P. H. Kobrin, G. A. Schick, J. Singh, J. P. Baxter, and B. J. Garrison, Surf. Sci. **176**, L817 (1986).
[40] S. W. Rosencrance, J. S. Burnham, D. E. Sanders, C. He, B. J. Garrison, and N. Winograd, Phys. Rev. B **52**, 6006 (1995).
[41] D. E. Sanders, P. B. S. Kodali, J. S. Burnham, and B. J. Garrison, Phys. Rev. B **50**, 5358 (1994).
[42] R. Smith, D. E. Harrison Jr., and B. J. Garrison, Phys. Rev. B **40**, 93 (1989).
[43] S. H. Goss, P. B. S. Kodali, B. J. Garrison, and N. Winograd, Surf. Sci. **387**, 44 (1997).
[44] B. J. Garrison, Chem. Soc. Rev. **21**, 155 (1992).
[45] R. Blumenthal, K. P. Caffey, E. Furman, B. J. Garrison, and N. Winograd, Phys. Rev. B **44**, 12 830 (1991).